Oudah, Mohamed; Takegami, Daisuke; Kitao, Shinji; Lado, Jose; Meléndez-Sans, Anna; Christovam, Denise S.; Yoshimura, Masato; Tsuei, Ku-Ding; McNally, Graham; Isobe, Masahiko; Küster, Kathrin; Seto, M.; Keimer, Bernhard; Bonn, D. A.; Tjeng, Liu Hao; Sawatzky, George; Takagi, Hidenori

Charge-entropy-stabilized selenide AgxSn1−xSe

Published in:
Communications Materials

DOI:
10.1038/s43246-025-00778-3

Published: 31/03/2025

Document Version
Publisher's PDF, also known as Version of record

communications materials

A Nature Portfolio journal

Article

https://doi.org/10.1038/s43246-025-00778-3

Charge-entropy-stabilized selenide $Ag_xSn_{1-x}Se$

Mohamed Oudah[1,2] ✉, Daisuke Takegami[3,4], Shinji Kitao[5], Jose L. Lado[6], Anna Meléndez-Sans[3], Denise S. Christovam[3], Masato Yoshimura[7], Ku-Ding Tsuei[7], Graham McNally[1], Masahiko Isobe[1], Kathrin Küster[1], M. Seto[5], Bernhard Keimer[1], D. A. Bonn[2], Liu Hao Tjeng[3], George Sawatzky[2] & Hidenori Takagi[1,8]

Configurational entropy has been discussed for high entropy alloys and high entropy oxides with multiple metal atoms sharing the same atomic site, where the entropy allows for the stability of a single phase material. Typically, the entropy from individual atoms occupying the same site is considered, but here we expand on this to include the entropy coming from charges on the cations sharing the same site. Considering the valence skip nature of Sn, the charge-entropy picture supports the stability region of rocksalt $Ag_xSn_{1-x}Se$. We find evidence for strong hybridization of the fluctuating Sn state from x-ray photoemission and Mössbauer spectroscopy, where these fluctuations on Sn are maintained to low temperature, well into the superconducting state, due to the lack of long-range order between Ag/Sn atoms in the entropy-stabilized rocksalt structure. Our charge-entropy model expands on the considerations when designing entropy-stabilized materials and opens up the possibility of designing new superconducting materials containing valence-skip elements.

In the study of crystalline solids, an emphasis is often placed on the highest possible degree of crystalline order. Fewer elements and simple stoichiometry make things simpler. Defects are unavoidable evils to be minimized. Cation and anion substitutions are necessary evils, used for doping and for tuning properties. Recently though, a new kind of simplicity has emerged when sufficient disorder is introduced that high-symmetry structures are stabilized by entropic considerations. This emergence of high-symmetry structures when multiple metals share the same site has been extensively discussed in the context of high-entropy alloys (HEA), with five or more elements sharing a site[1,2]. HEA have attracted attention due to two factors: the stability of high-symmetry phases not stable with fewer number of elements on the same site, and the unique properties that emerge in these materials[2].

This has recently been expanded to high-entropy carbides[3–5], high-entropy oxides[6], and high-entropy fluorides[7], where a simple anionic sublattice coexists with a cation site shared by five or more cations. In all of these cases, entropy comes from different elements sharing the same site, where each distinct element contributes to the configurational entropy equally, resulting in the stability of high-symmetry phases at high temperature, when the entropy term dominates the enthalpy term in the Gibbs free energy, $\Delta G = \Delta H - T\Delta S$, resulting in a single phase that can be quenched to ambient conditions. Here we extend this idea into new territory by considering entropy coming from different charge states of the constituent elements. This opens a large range of possibilities by reducing the number of elements needed for entropy-stabilization to be relevant.

One way to introduce elements with different charge states is to use valence skip elements in materials with intermediate nominal oxidation. This is an important class of materials hosting phenomena such as superconductivity[8], negative thermal expansion[9], and the charge-Kondo effect[10,11]. Such materials come in two categories: one where the average valence is a fraction of an electron and one with an integer number average valence, where the difference between the most stable states is an even number of electrons. In the former, when the charge is modulated in space we find the development of charge ordering, and when modulated in time, we find valence fluctuations. In some materials, these can overlap and differ only in the temperature at which the state is stable[12]. In the case of a whole number average valence, we find the emergence of disproportionation of ions into different sites, typically thought of as charge disproportionation[8]. Depending on the relative effective charge-transfer energy of the cation and valence band energy of the anion the electron may be shared along a

[1]Max Planck Institute for Solid State Research, Stuttgart, Germany. [2]Stewart Blusson Quantum Matter Institute, University of British Columbia, Vancouver, BC, Canada. [3]Max Planck Institute for Chemical Physics of Solids, Dresden, Germany. [4]Department of Applied Physics, Waseda University, Shinjuku, Tokyo, Japan. [5]Institute for Integrated Radiation and Nuclear Science, Kyoto University, Kumatori, Osaka, Japan. [6]Department of Applied Physics, Aalto University, Espoo, Finland. [7]National Synchrotron Radiation Research Center, Hsinchu, Taiwan. [8]Department of Physics, University of Tokyo, Bunkyo-ku, Tokyo, Japan. ✉e-mail: mohamed.oudah@ubc.ca

covalent bond between the cation and anion[13,14]. Two distinct crystallographic sites may arise resulting in a bond-disproportionated material with uniform cation charges and holes on the coordinating anions[15,16]. One can find fluctuations in these compounds by inducing a metallic state either through forced orbital overlap between neighboring atoms, by applying pressure, or the substitution of some elements to offset the whole number average charge such that a well-ordered lattice becomes unstable, leading to delocalization of the electrons.

Valence skip elements have stable oxidation states that vary by two charges where the middle oxidation state is not stable, such that $M^{(n-1)+}$ and $M^{(n+1)+}$ are stable, but the $M^{(n)+}$ is not stable or metastable. Materials with valence skip elements, such as Au, Tl, Sn, Pb, Sb, Bi, can have a whole number average nominal oxidation[8]. An insulating disproportionated state can emerge when we have an ordering of the charges, such is the case of $Ba_2Bi^{3+}Bi^{5+}O_6$[17] and $Cs_2Au^{1+}Au^{3+}Br_6$[18]. If the ordering of charges is destabilized, then electrons are delocalized, and electron conduction involves two-electron valence fluctuations on the valence skip element in these materials. These valence fluctuations have long been discussed in relation to superconductivity, where they are thought to contribute to pairing interactions through correlation-enhanced electron-phonon interaction[19] or negative-U superconductivity[8,20]. Here we consider the fluctuations on Sn in (Ag,Sn)Se, and the effect they have on the superconductivity and the stability of the cubic rocksalt structure. The role of charge and bond entropy in the stability of solids has been previously considered for Li_xFePO_4[21] and $LiNiO_2$[22], but the definitive role of charge/bond entropy in stabilizing a single phase remains an open question. We consider charge entropy on the Ag/Sn site in (Ag,Sn)Se, and the role of charge entropy in stabilizing the cubic structure. Unlike the high-entropy alloys and oxides, with five cations sharing the same site, a discussion of distinct ionic states when we consider two constituent elements is a simpler problem to solve.

We relate the charge-entropy in relation to the Sn-fluctuations to the stability of the rocksalt structure in $Ag_xSn_{1-x}Se$. X-ray photoemission spectroscopy (XPS) reveals a single peak with constant binding energy regardless of the composition x and a small shoulder at higher energy that increases in intensity with increasing x. Strong hybridization of Se-p and Sn-d, consistent with our DFT calculations, allows for a shift in spectral weight to the lower energy peak in our XPS spectra. We find evidence of a single distinct peak in the Sn-Mössbauer spectra for each composition of (Ag,Sn)Se down to 4 K. However, the position of this peak shifts for different samples with different composition of Ag in $Ag_xSn_{1-x}Se$, consistent with the average oxidation moving towards Sn^{2+} as x approaches zero. We provide a statistical argument for the distribution of Sn^{2+} and Sn^{4+} for a particular composition x to explain the shifting of the Sn-Mössbauer peak in each of the samples.

Results

Rocksalt $Ag_xSn_{1-x}Se$ and the state of Sn

$Ag_xSn_{1-x}Se$ is stable in the rocksalt structure for $0.38 \le x \le 0.50$, shown in Fig. 1(a), where the lattice constant a increases with increasing Sn content[23]. To obtain single phase samples it is necessary to quench from high-temperature[23]. Superconductivity is found in all $Ag_xSn_{1-x}Se$ samples in the rocksalt structure, where the T_c increases with higher Sn content, smaller x[24]. We attempt the synthesis of samples with higher Sn content with the aid of high-pressure high-temperature synthesis, but are unable to extend the stability of $Ag_xSn_{1-x}Se$ for $x \le 0.38$ even under high-pressure conditions. We find the same trend of increasing lattice constant and T_c with increasing Sn content in high-pressure grown samples as shown in the Supplemental Material, Fig. S5 ($T_c = 6.0$ K for $x = 0.38$, $T_c = 4.0$ K for $x = 0.50$). Fluctuations inside the superconducting state have been reported in $Ag_xSn_{1-x}Se$ for $x = 0.50$, with evidence of field-induced quantum fluctuations observed in resistivity measurements at low temperature[25].

Earlier work on the Sn Mössbauer of $Ag_xSn_{1-x}Se$ with different compositions demonstrates a peak that lies between that expected for 2+ and 4+ state[26], and this was explained by fluctuations of the Sn state where the Mössbauer probes the average of these two states due to the fast fluctuations relative to the energy difference of the probed states in Mössbauer[26,27]. A similar situation is expected when probing the states with NMR, where indeed a single peak is observed for $x = 0.5$ samples, which was attributed to a novel "Sn^{3+}" state[28]. Although it is reasonable considering the consistency of DFT calculations with the measured state in NMR[28], the calculations presented in the study only rule out the presence of a static charge disproportionation into differentiated sites. Furthermore, the study lacks any discussion of dependence of the Sn state on composition x and ignores previous XPS work demonstrating two distinct states for samples with different Sn content.

We bring to attention the importance of the stability region $0.38 \le x \le 0.5$ for the rocksalt structure of $Ag_xSn_{1-x}Se$, and relate this to the state of Sn in the material in Section "Charge-Entropy in $Ag_xSn_{1-x}Se$". In Section "XPS on $Ag_xSn_{1-x}Se$" we discuss the oxidation state of Sn in the same samples measured with XPS, and in Section "Low-temperature Mossbauer on $Ag_xSn_{1-x}Se$" we discuss the state measured with Mössbauer spectroscopy. Mössbauer measurements were carried out at low temperature showing persistent fluctuations down to 4 K, which has implications for the superconductivity.

Charge-entropy in $Ag_xSn_{1-x}Se$

We consider the entropy in the system as discussed for high-entropy alloys and compounds with the equation for configurational entropy S[1,29]. Here we utilize the idea of configurational entropy, and first consider the entropy on

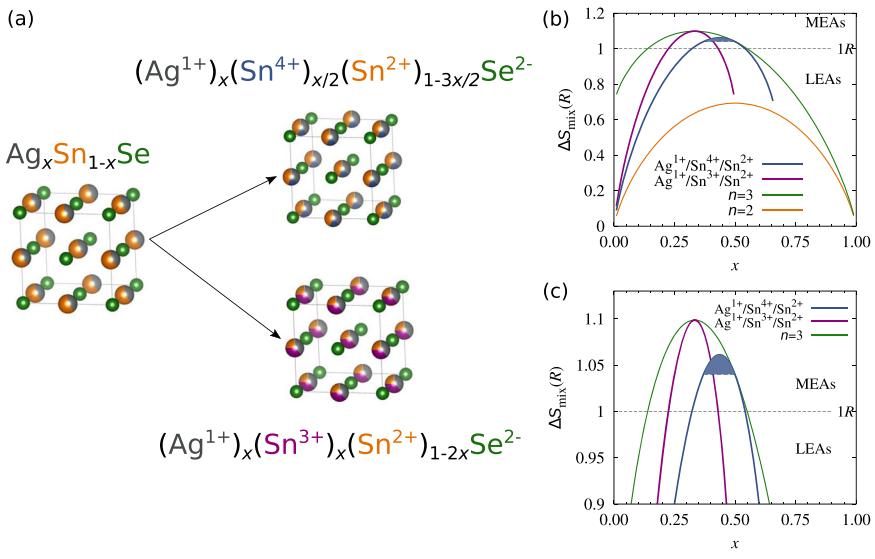

Fig. 1 | Entropy of cation site in rocksalt structure (Ag,Sn)Se^{2-}. **a** The rocksalt structure of (Ag,Sn)Se shown on the left side, and the two possible charge distributions on the Ag/Sn site are shown on the right. Top right shows the Sn^{2+}/Sn^{4+} distribution, and bottom right shows the Sn^{2+}/Sn^{3+} distribution, along the formulae dependence on x. **b** The entropy of mixing δS_{mix} for different numbers of components, $n = 2, 3$, sharing the same site as a function x for a single component with all other components being equal. The mixing δS_{mix} considering the charge entropy as a function of x for the case of $Sn^{2+}/Sn^{4+}/Ag^{+1}$ and $Sn^{2+}/Sn^{3+}/Ag^{+1}$ are shown for comparison. **c** A zoomed in result of (**b**) where the stability region of $Ag_xSn_{1-x}Se$ is highlighted with filled region around the peak of the curve for $Sn^{2+}/Sn^{4+}/Ag^{+1}$ entropy.

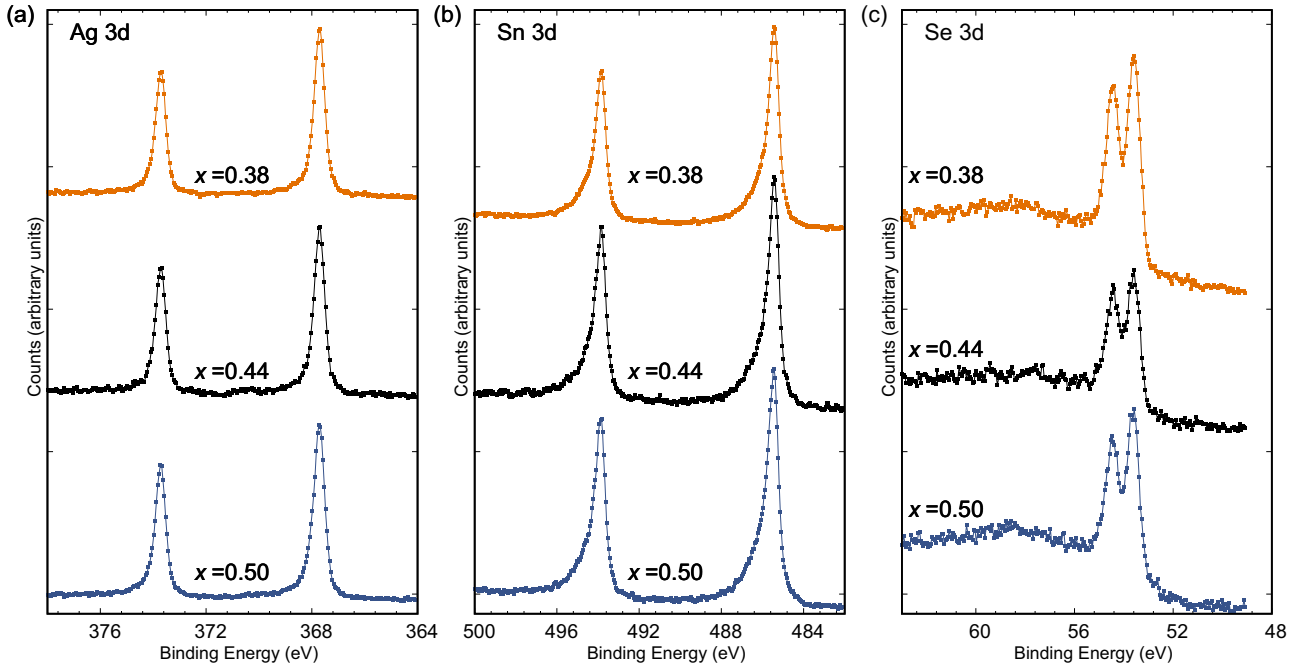

Fig. 2 | Bulk-sensitive x-ray photoemission spectra. Hard x-ray photoemission spectra of Ag, Sn, and Se in cleaved $Ag_xSn_{1-x}Se$ samples are shown in (**a**–**c**). The splitting between the main peaks is consistent with that expected due to spin-orbit-coupling (SOC) for the Ag, Sn, and Se 3*d* states, respectively.

the cation site coming from two distinct atoms in the case of $Ag_xSn_{1-x}Se$:

$$\Delta S_{\text{atom}} = R[xln(x) + (1-x)ln(1-x)] \quad (1)$$

where x is the composition of Ag. This is plotted with a orange curve ($n = 2$) in Fig. 1(b). For comparison, we examine the entropy from three constituent cations ($n = 3$) on the same site, where x corresponds to the content of one component while the other two components have equal composition with the green curve ($n = 3$) in Fig. 1(b).

Going beyond the entropy coming from the individual atomic species on the cation sites, we examine the charge-entropy. By considering two charge states on Sn we are simultaneously tuning three parameters, albeit coupled, by adjusting the Ag composition x. The charge-entropy on the cation site depends on the composition of Ag in the sample and the resulting Sn states in the two fluctuation scenarios. Pauli paramagnetism in $Ag_xSn_{1-x}Se$ would be much larger for Sn^{3+} with its unpaired electron, but we find the susceptibility to be fairly small, providing strong evidence for 2+/4+ fluctuations[27]. Nevertheless, we have considered two scenarios for the charge-entropy in $Ag_xSn_{1-x}Se$.

If we take the $x = 0.5$ sample as representing that of a true Sn^{3+} state, then as we increase the amount of Sn in the sample we must have an increase in the Sn^{2+} in the sample. The amount of Ag^{1+} and Sn^{3+} must be equal, such that the average charge of one Ag^{1+} and one Sn^{3+} is 2 + to balance with Se^{2-} anions, while the remaining Sn will be in the 2+ state. For this case of Sn^{3+}/Sn^{2+} fluctuations we have the following charge-entropy, $\Delta S_{Sn^{2+}/Sn^{3+}}$, dependence on the Ag-content x:

$$\Delta S_{Sn^{2+}/Sn^{3+}} = R[xln(x) + xln(x) + (1-2x)ln(1-2x)] \quad (2)$$

where the first and second term correspond to the entropy from Ag^{1+} and Sn^{3+}, while the third term corresponds to the entropy from Sn^{2+}.

The more likely scenario considering the low paramagnetism, is the 4+/2+ fluctuations. Here, the amount of Sn^{4+} in the sample corresponds to half the amount of Ag^{1+}, such that the average charge of one Sn^{4+} cation and two Ag^{+1} is 2+ to balance with Se^{2-} anions, while the remaining Sn atoms are Sn^{2+}. For the case of Sn^{4+}/Sn^{2+} we have the following charge-entropy, $\Delta S_{Sn^{2+}/Sn^{4+}}$, dependence on x:

$$\Delta S_{Sn^{2+}/Sn^{4+}} = R\left[xln(x) + \left(\frac{x}{2}\right)ln\left(\frac{x}{2}\right) + \left(1-\frac{3x}{2}\right)ln\left(1-\frac{3x}{2}\right)\right] \quad (3)$$

where the first term corresponds to the entropy from Ag^{1+}, the second term is for entropy from Sn^{4+}, and the third term corresponds to the entropy from Sn^{2+}.

In Fig. 1(a) and (b), we compare the curves for $\Delta S_{Sn^{2+}/Sn^{3+}}$ (purple curve) and $\Delta S_{Sn^{2+}/Sn^{4+}}$ (blue curve). We find that each curve representing the charge-entropy touches at one point the curve for the configurational entropy of a 3-component system ($n = 3$) defined above. However, the maximum entropy for the $\Delta S_{Sn^{2+}/Sn^{3+}}$ curve coincides with the maximum of the 3-component curve at $x = 0.33$, while the maximum of the $\Delta S_{Sn^{2+}/Sn^{4+}}$ curve is pushed to higher value of $x = 0.436$. The maximum entropy reached in $\Delta S_{Sn^{2+}/Sn^{4+}}$ is lower than that of $\Delta S_{Sn^{2+}/Sn^{3+}}$. However, the stability region for $Ag_xSn_{1-x}Se$ coincides well with the peak of the charge-entropy based on the 2+/4+ fluctuation scenario, $\Delta S_{Sn^{2+}/Sn^{4+}}$. We highlight the stability region of x around the maximum of the curve. Furthermore, quenching from high-temperature is important to stabilize a single phase sample as previously mentioned. This strongly hints at the stability of the phase being related to the domination of the entropy term at high temperature in the Gibbs free energy. Next, let us compare the observed oxidation state of Sn from XPS and Mössbauer spectroscopy.

XPS on $Ag_xSn_{1-x}Se$

In Fig. 2 we show the core level spectra of the $Ag_xSn_{1-x}Se$ samples measured on cleaved surfaces with hard x-ray photoelectron spectroscopy (HAXPES), in order to obtain results representative of the bulk of the compound. For both Ag 3*d* and Sn 3*d* we observe single sharp assymetric peaks, split by the spin orbit coupling (SOC). As for the Se 3*d*, we observe a clear two peak structure overlapping due to the smaller SOC of the Se 3d of around 1 eV. In order to understand better the trends in the spectral lineshape as well as position, we show a close-up comparison with normalized intensity of the Sn and Ag $3d_{5/2}$ spectra in Fig. 3.

First, we observe in Fig. 3(a) that the asymmetry of the Ag $3d_{5/2}$ peaks fully matches that of Ag metal (obtained from[30], shifted in energy to match

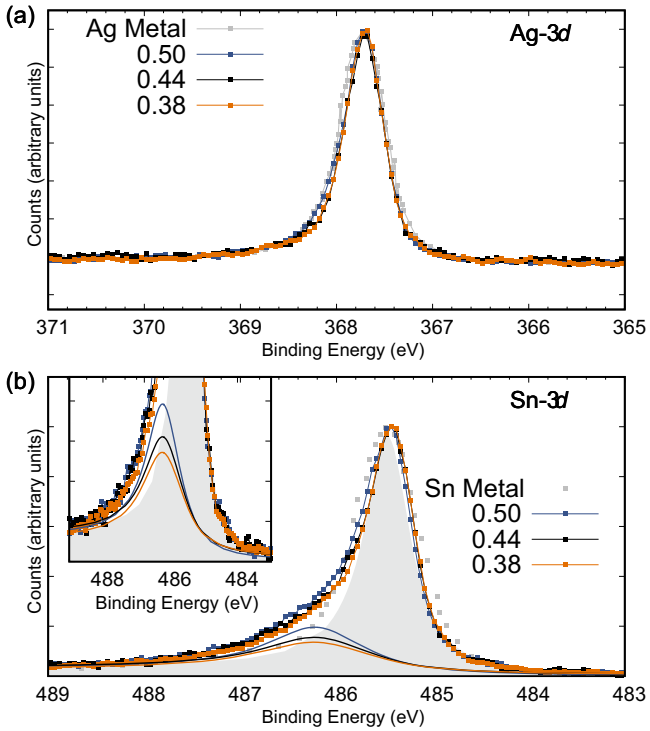

Fig. 3 | Comparison of cation photoemission spectra. Close-up of the hard x-ray photoemission spectra of the Ag-3$d_{5/2}$ (**a**) (Sn-3$d_{5/2}$) (**b**) in cleaved $Ag_xSn_{1-x}Se$ samples, normalized to their maximum intensities, together with the spectra from metallic Ag (Sn) from refs. 30, 31 shifted in binding energy to match the peak positions of $Ag_xSn_{1-x}Se$ in order to provide a comparison of the spectral lineshape.

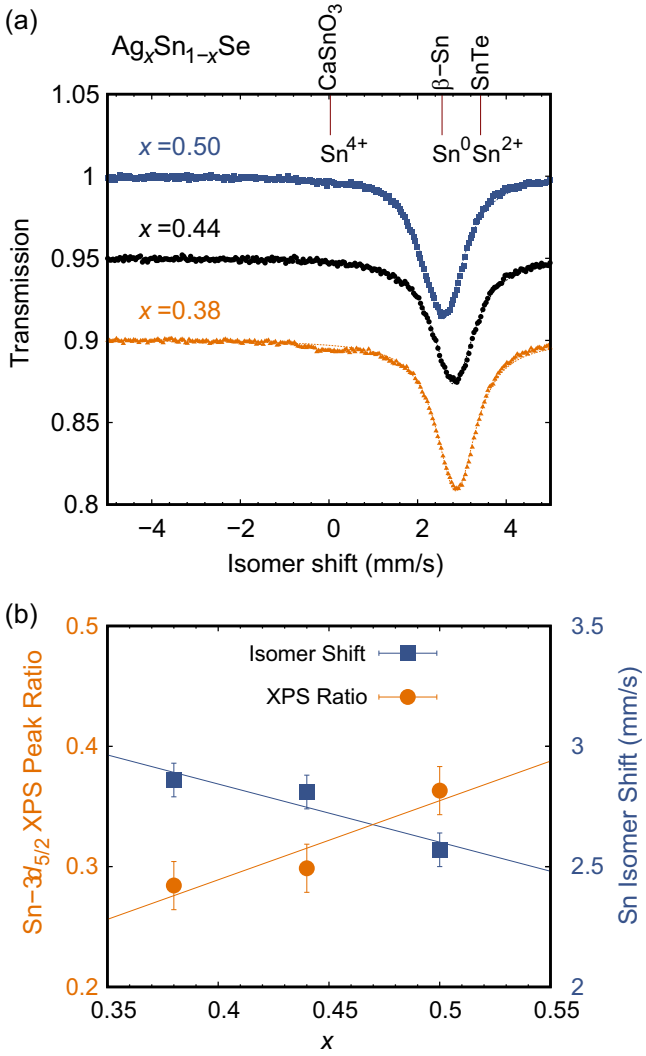

Fig. 4 | Mössbauer spectra and the average Sn state as a function of composition *x*. **a** The Mössbauer spectra of $Ag_xSn_{1-x}Se$ samples with different Ag-content, *x*. The spectra were measured at room temperature, and we found a shift in the peak position with Ag/Sn ratio in the samples. For $x = 0.5$ sample we find the peak in the isomer shift lies between that expected for 2+ and 4+, while an increase in Sn-content shifts the peak position towards that expected for a 2+ oxidation state. **b** The Ag-content, *x* in $Ag_xSn_{1-x}Se$, dependence of the ratio of the Sn-3$d_{5/2}$ fitted peaks in XPS and the isomer shift of Sn in Mössbauer spectra. A clear trend is observed in both as a function of *x*.

the peak position of the $Ag_xSn_{1-x}Se$ spectra), as could be expected from the metallicity of the system with strong contributions from all Ag, Sn and Se at the Fermi level, as shown in Fig. S7 of Supplemental Material. The position of the peak remains constant in energy for all *x*. Thus, our Ag 3*d* core level spectra are consistent with a single valent Ag^{1+} metallic state that remains stable with increasing *x*.

As for the Sn 3$d_{5/2}$ (Fig. 3(b)), we observe that while most of its spectral weight can be explained by the Doniach-Sunjich asymmetric shape as seen in Sn metal (obtained from[31], shifted in energy to match the peak position of the $Ag_xSn_{1-x}Se$ spectra), there is an additional small component at around 486.5 eV. The single dominant component in the core level spectra rules out the possibility of a static (e.g., ordered) charge disproportionate, where 2 separate peaks from the Sn^{2+} and Sn^{4+} with spectral weight ratios directly reflecting their proportion in the ground state would be expected. Instead, it indicates that the Sn ions must be either all single valent or highly fluctuating state.

Under a single valent assumption, one would expect the nominal valence changes of Sn resulting from changing *x*, from 3+ to around 2.6+, to be reflected in a core level energy position shift. However, the Sn 3*d* peak remains in all cases at a constant position within our experimental resolution, ruling out also this possibility. This leaves us with the highly fluctuating valence scenario, with a fluctuation of two electrons due to an effective attractive *U* on the Sn atoms[8]. Considering the Robin-Day classification scheme[32], $Ag_xSn_{1-x}Se$ falls into class IIIB where even a fast technique such as HAXPES does not show two distinct peaks corresponding to two distinct states.

Nevertheless, the presence of the additional component observed at around 486.5 eV matches with the expected "antibonding" peak that would arise from the two fluctuating states, as discussed in more detail in Supplemental Material, Sec. A. In particular, we observe that the experimental spectra can be well described by a fixed main Doniach-Sunjic peak at 485.5 eV and a small second contribution at 486.5 eV, as highlighted in the inset of Fig. 3(b), which systematically increases as a function of x (Fig. 4(b)), in agreement with the behavior predicted for the "antibonding" peak in the qualitative core level model presented in Supplemental Material, Sec. A.

The core level spectra discussed in this section differ significantly from those reported in the literature[33], where additional components are observed both in the Sn 3*d* as well as Se 3*d*. In order to understand the reported differences, we present the XPS spectra on as-grown uncleaved surfaces in Supplemental Material, Fig. S1. While the Ag 3*d* results are similar to those obtained on the cleaved samples with HAXPES, the Sn 3*d* as well as Se 3*d* show significantly different spectral lineshapes. In the Sn 3*d* we observe a clear 2-component structure, with one peak at around 485.5 eV that would correspond to the bulk contribution observed in the cleaved HAXPES measurements, and a new, larger component at around 487.2 eV. The binding energy of this second larger component clearly differs from the 486.5 eV component discussed above, indicating the 487.2 eV peak in the uncleaved XPS spectra is not a mere change in the Sn^{2+}-Sn^{4+} behavior but rather arises from a new contribution not present in the cleaved HAXPES

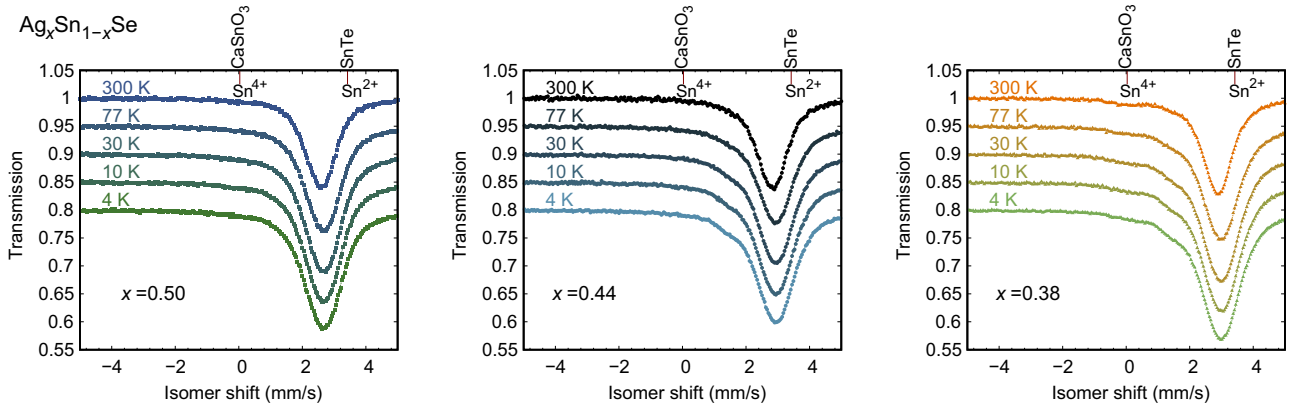

Fig. 5 | Low temperature Mössbauer spectra of Sn for different *x*. The Mössbauer spectra of $Ag_xSn_{1-x}Se$ samples with different Ag-content, for x = 0.50, 0.44, 0.38 from left to right. An increase in Sn-content shifts the peak position towards that expected for a 2+ oxidation state. The spectra were measured at different temperatures down to 4 K, and we find a single dominant peak position for all x values down to 4 K.

measurements, namely the oxidized surface. Similarly, in the Se 3*d*, the experimental spectra no longer display the clear two SOC-split structure, but instead, have a more complex shape resulting from one additional set of surface components mixed in. These results indicate that the surface stability is affected by the Ag/Sn ratio in the samples, which results in different levels of surface oxidation and a different ratio of the surface to bulk peaks depending on x. As such, bulk-sensitive measurements on fresh, clean surfaces are crucial to obtain results representative of the intrinsic electronic structure of $Ag_xSn_{1-x}Se$.

Low-temperature Mössbauer on $Ag_xSn_{1-x}Se$

The Sn-Mössbauer for $Ag_xSn_{1-x}Se$ samples with different x are shown in Fig. 4(a), where we find a single peak for each composition x. The isomer shift of $Ag_xSn_{1-x}Se$ corresponds to an intermediate state between divalent and quadrivalent-tin compounds. The Sn^{2+} and Sn^{4+} impurity ions in PbSe should be compared with the state in $Ag_xSn_{1-x}Se$ to allow for a comparison where the environment is that of 6-coordinated Se in all cases[27]. The position of the peak in the isomer shift moves to higher values with decreasing x, which suggests fluctuations between two different states of Sn where the Mössbauer picks up the average of these fluctuations. The shift with composition suggests an increase in 2+ contribution to the fluctuations on average resulting in the position moving towards that of Sn^{2+}, such is the state in SnTe[27]. This further supports the nature of the fluctuations deduced from the stability region, as discussed in Section "Charge-Entropy in $Ag_xSn_{1-x}Se$".

Mössbauer level lifetime determines the natural spectral-line width, which is $G_{nat} = h/t_0 = 0.324$mm/s for Sn. The experimental width always exceeds $2G_{nat}$, where the broadening is attributed to unresolved quadrupole splitting, finite absorber surface density, and electron exchange between two tin-charge states. Fluctuations on Sn in $Ag_xSn_{1-x}Se$ may be related to an activation energy, where the lifetime of each Sn increases such that $t >> t_0$. In such a scenario, a single peak at high temperature should split into two peaks corresponding to each of these states. The slowing down of fluctuations and splitting of Mössbauer spectra has been observed in Eu_3S_4, where a single peak in the isomer shift at room temperature splits into peaks corresponding to 2+ and 3+ at low temperature[34]. We compare as a function of x the isomer shift and the relative peak ratio in XPS in Fig. 4(b), and we find a decrease in the isomer shift and an increase in the relative peak ratio as expected for an increase in Sn^{4+} contribution with increasing x.

We measure the Mössbauer spectra of three different samples, with x = 0.38, 0.44, and 0.50, down to 4.0 K. Comparing the Mössbauer spectra at room temperature for all three compositions in Fig. 4(a), we find the isomer shift decreases with increasing x. For all three samples, a single peak is observed down to 4.0 K, shown in Fig. 5, which means that if the peak position is a consequence of fluctuations, then these fluctuations persist down to 4.0 K. We do find some evidence for peak broadening at low temperature, and we fit the low temperature Mössbauer spectra to multiple peaks as shown in Supplemental Material, Fig. S3. The change in the isomer shift as a function of temperature, shown in Supplemental Material, Fig. S4, shows no evidence of a splitting of one peak into two peaks with the slowing down of fluctuations, as seen in Eu_3S_4[34]. This is likely related to the disorder, lack of long range order, of Ag and Sn on the same site of $Ag_xSn_{1-x}Se$, which hinders the distortion of the structure in a lower symmetry structure to localize the Sn^{2+} and Sn^{4+} states.

Using DFT simulations, we find that forcing different charges on Sn atoms in ordered lattices, followed by allowing the relaxation of the structure and the charge results in redistribution to almost equal charge on all Sn atoms. This hints at strong correlation in (Ag,Sn)Se evident by the shift of spectral weight in the Sn XPS from the higher binding energy peak to the lower binding energy. Also, we have performed calculations on supercells with disordered Ag and Sn atoms, and find the charge on all atoms varies within $\pm 0.1e$ for different Ag:Sn ratios, as shown in Supplemental Material, Fig. S6.

We consider the statistical distribution of the nearest neighbor and next-nearest neighbor atoms to explain the shift in the position of the isomer shift of fluctuating Sn with x, as demonstrated in Fig. 6. With a Se^{2-} lattice and constrained by Ag^{+1}, we consider the effect of randomly distributed Ag/Sn on the likelihood of the central Sn being in the 4+ or 2+ state. We examine the nearest neighbor Se atoms bonded to Sn, n, (Fig. 6(a)) and next-nearest neighbor Ag/Sn atoms, n', (Fig. 6(b)) around a center Sn atom. For the case of high n/n' on the right side of Fig. 6(a) and (b) we expect a Sn^{2+} state, and for the case of low n/n' we expect a Sn^{4+} state. We compare the statistical distribution for the case of x = 0.50 and x = 0.38, and we find a higher Sn^{2+} state contribution to the fluctuations for the lower Ag content (x = 0.38) as expected, consistent with the change in the isomer shift in Mössbauer. We note that the x = 0.50 sample (T_c = 6.0 K) is well inside the superconducting state at 4.0 K, which suggests that these fluctuations on Sn persist inside the superconducting state. If these fluctuations on Sn are important to the emergence of superconductivity, then they may be related to the quantum fluctuations previously reported in resistivity measurements[25].

We consider the degree of short-range order (SRO) in $Ag_xSn_{1-x}Se$ associated with fluctuations on Sn. We find that SnSe distorts into an orthorhombic phase *Pnma* due to the lone-pair on Sn^{2+} ions[35]. However, the addition of Ag in $Ag_xSn_{1-x}Se$ results in cation site being occupied by two cation species without lone-pairs, Ag^{1+} and Sn^{4+}, that limit distortion of the structure due to the remaining Sn^{2+} ions. Local distortions associated with the Sn^{2+} ions in $Ag_xSn_{1-x}Se$ may be present and should be investigated in future studies that consider the degree of SRO. The degree of SRO can be quantified by evaluating the Warren-Cowley parameters typically discussed for disordered alloys[36,37]. The emergence of SRO in rocksalt

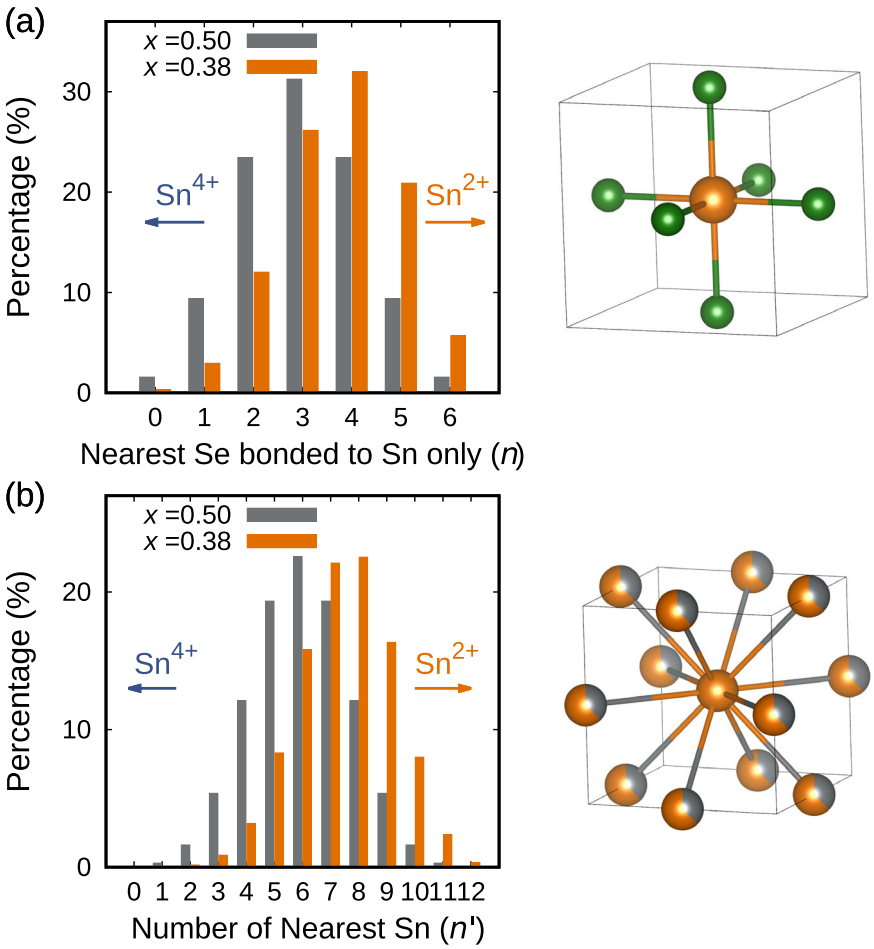

Fig. 6 | Statistical distribution of Sn environment for different *x*. **a** Statistical distribution of the environment of Sn environment, where we consider the nearest Se atoms and whether they are bonded to Sn or Ag. Based on the value *x* for Ag/Sn, we find a shift in the distribution of bonded Se atoms moving the distribution towards Sn^{2+} for smaller *x*. **b** Similar statistical analysis as (**a**), but considering the next-nearest Ag/Sn distribution around the center Sn atom. More Sn^{2+} like state is expected for more Sn in the environment.

PbTe at high temperature[38] and the Ni-Ni bonding driven SRO in $KNiSe_2$[39] also at high temperature will be interesting to compare with $Ag_xSn_{1-x}Se$. These investigations will deepen our understanding of a single-phase rocksalt structure the emerges from cation disorder on a single crystallographic site.

Conclusion

We report the HAXPES of $Ag_xSn_{1-x}Se$, where for all *x* values a single symmetric peak with constant energy is found for the Ag-3*d* spectra and a single peak with constant energy maximum and varying asymmetry in the Sn-3*d* spectra. We find that the degree of asymmetry varies as a function of *x* consistent with a change in the ratio of Sn^{2+} to Sn^{4+}, where higher Sn^{4+} is expected for higher *x*. In contrast, the isomer shift in the Mössbauer spectra shows a single peak that shifts towards the value of Sn^{4+} with increasing *x*. Taking the single peak in the HAXPES for Ag-3*d* as evidence for a Ag^{+1}, we evaluate the charge entropy from cation species in $Ag_xSn_{1-x}Se$ considering the three cation species. We compare the charge entropy as a function of *x* considering these three cations $Ag^{+1}/Sn^{2+}/Sn^{4+}$ and compare this with the model for having $Ag^{+1}/Sn^{2+}/Sn^{3+}$, and find that the highest entropy region for the former model coincides with the stability region ranging from 0.38 to 0.5 for *x* of $Ag_xSn_{1-x}Se$.

The stability region of $Ag_xSn_{1-x}Se$ demonstrates that crystalline order can emerge from high charge disorder. We believe that the stability region of $Ag_xSn_{1-x}Se$ validates the Sn-fluctuations long suspected and the nature of the competition that gives rise to a correlated metal in the normal state. Furthermore, the consideration of charge-entropy in this valence skip compound is successful in explaining the formation of a single phase that can be quenched from high temperature, and opens up the possibility of exploiting the charge entropy in search of other phases that include valence skip elements. However, one should still consider the nature of the individual charged species when looking for new charge-entropy stabilized compounds, which can result in distortion of the high symmetry structure or the formation of an impurity phases that limit the applicability of the charge-entropy model.

Finally, the two-electron mechanism related to the negative-*U* on Sn is likely related to the superconductivity in $Ag_xSn_{1-x}Se$. One may even attribute the higher T_c in Sn-rich samples to a higher concentration of negative-*U* centers, but this will need further clarification with additional experiments. Once high crystalline order emerges the virtue of charge disorder results in a tension between charge states on the valence skip atoms that can promote superconductivity.

Methods

Synthesis and basic characterization

$Ag_xSn_{1-x}Se$ samples were synthesized with a high-pressure, high-temperature method utilizing a belt-press. Ag, Sn, and Se powders were well mixed in a mortar and pestle, then loaded into a gold capsule. The capsule was then pressed to 6 GPa and heated at 730 K for 1 hour before quenching and retrieving the polycrystalline product. A finely ground sample was loaded into a 0.3 mm capillary, and powder x-ray diffraction (XRD) patterns of $Ag_xSn_{1-x}Se$ were collected while rotating the capillary using Ag radiation (0.5594 Å). Samples synthesized under high-pressure were used for Mössbauer and XPS measurements. $Ag_xSn_{1-x}Se$ samples for HAXPES measurements were synthesized using Bridgman method by placing the elements Ag,Sn, and Se in different ratios for each *x* in vacuum-sealed tube that were sealed inside another tube and heated to 1000 °C over 15 h and remaining at 1000 °C for 40 h. Then the tube was cooled to 450 °C at the rate of 3 °C/h, followed by quenching the tubes in air.

Mössbauer spectroscopy

Mössbauer was performed using a $CaSnO_3$ with ^{119m}Sn as the γ-ray source (Ritverc GmbH, 740 MBq). The absorption of ^{57}Fe was used to calibrate the velocity of the source, and the isomer shift of $BaSnO_3$ at room temperature was set as the origin. A 75 μm thick palladium film was placed between the source and the sample in order block the x-ray fluorescence of Sn. The synthesized samples were first characterized using X-ray diffraction and magnetization measurements. The sample was ground into a powder (~ 50 mg) and mixed under nitrogen atmosphere with boron nitride powder (~ 70 mg, Kishida Chemical, 99.5%) and polyethylene powder (~ 8 mg Beckman RIIC, polyethylene powder for IR spectroscopy) to improve the homogeneity of the sample. Then the sample was pressed into a pellet (10 mm diameter). All measurements, from room temperature down to 4 K, were carried out inside a ^4He cryostat (Janis Research, ST-400). The time for each measurement was about 12 h.

X-ray photoemission

The XPS data on uncleaved samples were collected using a commercial Kratos AXIS Ultra spectrometer and a monochromatized Al K_α source (photon energy: 1486.6 eV). The base pressure during XPS was in the low 10^{-10} mbar range. The spectra were collected using an analyzer pass energy of 20 eV. XPS spectra were analyzed using the CasaXPS software. To fit the peaks, a combination of multiple Gaussian-Lorentzian mixture functions and a Shirley background was used. For the Ag-3*d* and the Sn-3*d* the binding energy separation and the area ratio of the doublets were not constrained, but the results are within experimental error of the tabulated values[40], while for the Se-3$d_{5/2}$ and Se-3*d*3/2 the binding energy separation and area ratio were constrained to 0.86 eV and 3:2, receptively. The sum of all the fitted functions to XPS peaks is shown with a black curve in Supplemental Material, Fig. S1.

The HAXPES data on cleaved samples were collected at the Max-Planck-NSRRC HAXPES end-station at the Taiwan undulator beamline BL12XU at SPring-8, Japan[41] using an MB Scientific A-1 HE analyzer. The photon beam was linearly polarized with the electrical field vector in the plane of the storage ring (i.e., horizontal), and the photon energy was set at about 6.5 keV, with an overall energy resolution of around 280 meV, determined by measuring an Au reference sample. The samples were cleaved in a preparation chamber adjacent at a base pressure in the low 10^{-9} mbar, and transferred in-situ to the measuring chamber, where the base pressure was in the low 10^{-10} mbar.

Density functional theory

Electronic structure calculations were performed within the framework of density functional theory (DFT) as implemented in the Quantum Espresso package[42]. The generalized gradient approximation with the PBEsol for the exchange-correlation functional was used[43,44] and PAW pseudopotentials. Calculations were converged with respect to the plane wave cutoff and reciprocal space grid. The face-centered cubic crystal structure ($a = 5.675$ Å) was used[23]. We performed calculations on large supercells ($3 \times 3 \times 3$) with disordered Ag and Sn atoms, placed randomly with our own built Python code to generate a disordered supercell, to evaluate the distribution of charge on atoms.

Statistical methods

The statistical distribution of atoms was calculated using combination statistics[45]. We consider total number of cations to choose from t and x is percentage of Ag atoms in t. Then, the total number of Sn atoms is $s = t \times (1 - x)$ and total number of Ag atoms is $a = t \times x$. The probability P_n of n distinct surrounding atoms (nearest neighbor Se bonded to Sn or next-nearest neighbor Sn) around a central Sn atom is calculated with:

$$P_n = \frac{C(s,n) \times C(a,m)}{C(t,r)} \tag{4}$$

where r is total number of nearest/next-nearest atoms, such that $r = 6$ when considering nearest neighbor Se atoms and $r = 12$ when considering next-nearest neighbor Ag/Sn atoms. We consider integer values of n between 0 and r, and the number of remaining atoms (nearest-neighbor Se not bonded to Sn or next-nearest neighbor Ag) is $m = r - n$. C is the combination functions defined as $C(x,y) = \frac{x!}{y!(x-y)!}$. The calculation was repeated with increasing t until the calculated probability did not change to 3 significant digits.

Data availability

The authors declare data supporting the findings of this study are available within the paper and its Supplementary Information. A supercell of $Ag_xSn_{1-x}Se$ with random Ag/Sn is included as Supplementary Data 1. All data are available from the authors on reasonable request.

Received: 16 October 2024; Accepted: 5 March 2025;
Published online: 31 March 2025

References

1. Yeh, J.-W. et al. Nanostructured high-entropy alloys with multiple principal elements: novel alloy design concepts and outcomes. *Adv. Eng. Mater.* **6**, 299–303 (2004).
2. George, E. P., Raabe, D. & Ritchie, R. O. High-entropy alloys. *Nat. Rev. Mater.* **4**, 515–534 (2019).
3. Castle, E., Csanádi, T., Grasso, S., Dusza, J. & Reece, M. Processing and properties of high-entropy ultra-high temperature carbides. *Sci. Rep.* **8**, 8609 (2018).
4. Yan, X. et al. ($hf_{0.2}zr_{0.2}ta_{0.2}nb_{0.2}ti_{0.2}$)c high-entropy ceramics with low thermal conductivity. *J. Am. Ceram. Soc.* **101**, 4486–4491 (2018).
5. Sarker, P. et al. High-entropy high-hardness metal carbides discovered by entropy descriptors. *Nat. Commun.* **9**, 4980 (2018).
6. Rost, C. M. et al. Entropy-stabilized oxides. *Nat. Commun.* **6**, 8485 (2015).
7. Chen, X. & Wu, Y. High-entropy transparent fluoride laser ceramics. *J. Am. Ceram. Soc.* **103**, 750–756 (2020).
8. Varma, C. Missing valence states, diamagnetic insulators, and superconductors. *Phys. Rev. Lett.* **61**, 2713 (1988).
9. Takenaka, K. Progress of research in negative thermal expansion materials: paradigm shift in the control of thermal expansion. *Front. Chem.* **6**, 267 (2018).
10. Matsushita, Y., Bluhm, H., Geballe, T. & Fisher, I. Evidence for charge Kondo effect in superconducting TL-doped PbTe. *Phys. Rev. Lett.* **94**, 157002 (2005).
11. Matsuura, H., Mukuda, H. & Miyake, K. Valence skipping phenomena, charge kondo effect, and superconductivity. *AAPPS Bull.* **32**, 30 (2022).
12. Goto, T. & Lüthi, B. Charge ordering, charge fluctuations and lattice effects in strongly correlated electron systems. *Adv. Phys.* **52**, 67–118 (2003).
13. Zaanen, J., Sawatzky, G. & Allen, J. Band gaps and electronic structure of transition-metal compounds. *Phys. Rev. Lett.* **55**, 418 (1985).
14. Mizokawa, T. et al. Origin of the band gap in the negative charge-transfer-energy compound $NaCuO_2$. *Phys. Rev. Lett.* **67**, 1638 (1991).
15. Foyevtsova, K., Khazraie, A., Elfimov, I. & Sawatzky, G. A. Hybridization effects and bond disproportionation in the bismuth perovskites. *Phys. Rev. B* **91**, 121114 (2015).
16. Balandeh, S. et al. Experimental and theoretical study of the electronic structure of single-crystal $babio_3$. *Phys. Rev. B* **96**, 165127 (2017).
17. Rice, T. & Sneddon, L. Real-space and $\vec{k}$-space electron pairing in $bapb_{1-x}bi_xo_3$. *Phys. Rev. Lett.* **47**, 689 (1981).
18. Riggs, S. C. et al. Single crystal growth by self-flux method of the mixed valence gold halides Cs_2 [$Aau^{I}x_2$][$Au^{III}x_4$](x = Br, I). *J. Cryst. Growth* **355**, 13–16 (2012).
19. Kulić, M. L. Interplay of electron–phonon interaction and strong correlations: the possible way to high-temperature superconductivity. *Phys. Rep.* **338**, 1–264 (2000).

20. Anderson, P. Model for the electronic structure of amorphous semiconductors. *Phys. Rev. Lett.* **34**, 953 (1975).
21. Zhou, F., Maxisch, T. & Ceder, G. Configurational electronic entropy and the phase diagram of mixed-valence oxides: The case of Li_xFePo_4. *Phys. Rev. Lett.* **97**, 155704 (2006).
22. Foyevtsova, K., Elfimov, I., Rottler, J. & Sawatzky, G. A. Linio 2 as a high-entropy charge-and bond-disproportionated glass. *Phys. Rev. B* **100**, 165104 (2019).
23. Wold, A. & Brec, R. Structure NaCl des phases $Ag_xSn_{1-x}x(x = S, Se)$. *Mater. Res. Bull.* **11**, 761–765 (1976).
24. Johnston, D. & Adrian, H. Superconducting and normal state properties of $Ag_{1-x}Sn_{1+x}Se_{2-y}$. *J. Phys. Chem. Solids* **38**, 355–365 (1977).
25. Ren, Z. et al. Anomalous metallic state above the upper critical field of the conventional three-dimensional superconductor $AgSnSe_2$ with strong intrinsic disorder. *Phys. Rev. B* **87**, 064512 (2013).
26. Masterov, V. et al. Unconventional tin atom states in mixed silver and tin chalcogenides having NaCl structure. *Phys. Solid State* **38**, 1805–1806 (1996).
27. Nasredinov, F., Nemov, S., Masterov, V. & Seregin, P. Mössbauer studies of negative-*u* tin centers in lead chalcogenides. *Fiz. Tverd. Tela* **41**, 1897–1917 (1999).
28. Naijo, Y. et al. Unusual electronic state of Sn in $AgSnSe_2$. *Phys. Rev. B* **101**, 075134 (2020).
29. Swalin, R. A.*Thermodynamics of Solids*(New York: John Wiley & Sons) 2nd edn (1972).
30. Gegner, J. et al. Electronic structure of *r*AuMg and *r*AgMg (*r* = Eu, Gd, Yb). *Phys. Rev. B* **74**, 073102 (2006).
31. Fondell, M., Gorgoi, M., Boman, M. & Lindblad, A. An HAXPES study of Sn, SnS, SnO and Sn_2. *J. Electron Spectros. Relat. Phenom.* **195**, 195–199 (2014).
32. Robin, M. B. & Day, P. Mixed valence chemistry-a survey and classification. In *Adv. Inorg. Chem. Radiochem*., vol. 10, 247–422 (Elsevier, 1968).
33. Wakita, T. et al. The electronic structure of $Ag_{1-x}Sn_{1+x}Se_2$ (x = 0.0, 0.1, 0.2, 0.25 and 1.0). *Phys. Chem. Chem. Phys.* **19**, 26672–26678 (2017).
34. Berkooz, O., Malamud, M. & Shtrikman, S. Observation of electron hopping in $^{151}eu_3s_4$ by mössbauer spectroscopy. *Solid State Commun.* **6**, 185–188 (1968).
35. Wiedemeier, H., Georg, H. & Schnering, GV Refinement of the structures of ges, gese, sns and snse. *Z. für Kristallographie-Crystalline Mater.* **148**, 295–304 (1978).
36. Norman, N. & Warren, B. X-ray measurement of short range order in Ag-Au. *J. Appl. Phys.* **22**, 483–486 (1951).
37. Cowley, J. Short-range order and long-range order parameters. *Phys. Rev.* **138**, A1384 (1965).
38. Božin, E. S. et al. Entropically stabilized local dipole formation in lead chalcogenides. *Science* **330**, 1660–1663 (2010).
39. Neilson, J. R. et al. Dynamical bond formation in KNi_2Se_2. *Z. für Anorganische Allg. Chem.* **648**, e202200042 (2022).
40. Moulder, J. & Chastain, J. *Handbook of X-ray Photoelectron Spectroscopy: A Reference Book of Standard Spectra for Identification and Interpretation of XPS Data* (Physical Electronics Division, Perkin-Elmer Corporation, 1992).
41. Takegami, D. et al. Valence band hard x-ray photoelectron spectroscopy on 3*d* transition-metal oxides containing rare-earth elements. *Phys. Rev. B* **99**, 165101 (2019).
42. Giannozzi, P. et al. Quantum espresso: a modular and open-source software project for quantum simulations of materials. *J. Phys. Condens. Matter* **21**, 395502 (2009).
43. Perdew, J. P., Burke, K. & Wang, Y. Generalized gradient approximation for the exchange-correlation hole of a many-electron system. *Phys. Rev. B* **54**, 16533 (1996).
44. Perdew, J. P., Burke, K. & Ernzerhof, M. Generalized gradient approximation made simple. *Phys. Rev. Lett.* **77**, 3865–3868 (1996).
45. Harris, J. M. *Combinatorics and graph theory* (Springer, 2008).

Acknowledgements

We thank Faiza Bassiseau for help with statistics. We thank Manfred Sigrist for feedback on the manuscript. We thank Frank Falkenberg for assistance with high-pressure experiments. We thank Christine Stefani for assistance with XRD experiments. We thank the Max Planck-UBC-UTokyo Center for Quantum Materials for support. We acknowledge the support for the HAXPES measurements from the Max Planck-POSTECH-Hsinchu Center for Complex Phase Materials. D.T. acknowledges the support by the Deutsche Forschungsgemeinschaft (DFG, German Research Foundation) under the Walter Benjamin Programme, Projektnummer 521584902.

Author contributions

M.O. conceived of the charge-entropy idea. M.O., G.M., M.I., and H.T. synthesized samples under high-pressure high-temperature conditions. D.T. A.M.S., D.C., M.Y., K.D.T., H.T. performed HAXPES measurements. D.T. analyzed the HAXPES spectra with help from G.S. and H.T. S.K. and M.S. measured and analyzed the Mössbauer spectra. J.L.L. performed DFT calculations. K.K. measured and analyzed the XPS sepctra. M.O. synthesized samples with Bridgmann method with help from D.A.B. M.O. measured the magnetization of samples with help from B.K. M.O. performed statistical analysis with help from G.S. The manuscript was mainly written by M.O. and D.T. with help from D.A.B. and G.S. and feedback from other co-authors.

Funding

Open Access funding enabled and organized by Projekt DEAL.

Competing interests

The authors declare no competing interests.

Additional information

Supplementary information The online version contains supplementary material available at https://doi.org/10.1038/s43246-025-00778-3.

Correspondence and requests for materials should be addressed to Mohamed Oudah.

Peer review information *Communications Materials* thanks Akio Kimura, Tyrel McQueen, and the other anonymous reviewer(s) for their contribution to the peer review of this work. Primary Handling Editors: Kohei Fujiwara and Aldo Isidori.